ORIGINAL ARTICLE

Momentum and energy considerations in self-aerated free-surface flows

Hubert Chanson[1] · Yvan Aroquipa Nina[2]

Abstract

In high-velocity free-surface flows, the interactions between the fast-flowing flow and the atmosphere can lead to strong air–water mixing through the free-surface. The flow resistance may be derived from momentum and energy considerations. This was undertaken through some theoretical development based upon an extension of traditional integral approaches to air–water flows, with the re-analyses of detailed air–water measurements in both prototype spillways and large-size physical models. Both the momentum and energy approaches yielded close results in terms of the Darcy-Weisbach friction factor. Based upon the same data sets, the absence of correction coefficients was found to under-estimate the residual energy, compared to the detailed calculations using the relevant air–water kinetic energy and pressure correction coefficients. The finding has basic design implications, which are discussed.

Keywords Self-aerated flows · Free-surface flows · Momentum · Energy · Friction factor · Residual head · Dam spillways · Correction coefficients

Abbreviations

A	Clear-water flow area: herein $A = d \times B$;
B	Rectangular channel width (m);
C	Time-averaged void fraction;
C_{mean}	Depth-averaged void fraction ($C_{mean} = \frac{1}{Y_{90}} \times \int_{y=0}^{Y_{90}} C \times dy$)
D_H	Hydraulic diameter (m): $D_H = 4 \times A/P_w$;
d	Equivalent clear-water depth (m) in air–water flows ($d = \frac{1}{Y_{90}} \times \int_{y=0}^{Y_{90}} (1 - C) \times dy$)
d_c	Critical flow depth (m);
F_{drag}	Total drag force (N);
f	Darcy-Weisbach friction factor for air–water flow;
g	Gravity acceleration (m/s^2);
H	Total head (m);

✉ Hubert Chanson
     h.chanson@uq.edu.au

[1] Professor in Hydraulic Engineering, School of Civil Engineering, The University of Queensland, Brisbane, QLD 4072, Australia

[2] Research Student, School of Civil Engineering, The University of Queensland, Brisbane, QLD 4072, Australia

H_{res} Residual head (m);

h   Vertical step height (m), measured from step edge to step edge;

$\dot{KE}$ Rate of change of kinetic energy (J/s);

P   Pressure (Pa);

P_w Wetted perimeter (m);

Q   Water discharge (m^3/s);

q   Water discharge per unit width (m^2/s): $q = Q/B$;

Re   Reynolds number defined in terms of the mean velocity and hydraulic diameter ($Re = \rho \times \frac{V_{mean} \times D_H}{\mu}$)

$\dot{S}_f$ Friction slope;

U Rate of change of works associated to conservative forces (J/s);

V   Velocity (m/s);

V_{mean} Cross-sectional mean velocity (m/s): $V_{mean} = Q/A$;

V_x Longitudinal velocity component (m/s);

V_{90} Characteristic air–water velocity (m/s) where C=0.90;

W   Weight force (N);

x   Longitudinal distance (m) positive downstream;

Y_{90} Characteristic air–water elevation (m) where C=0.90;

y   Normal distance (m) measured perpendicular to and above the invert or pseudo-invert formed by the step edges;

z_o Invert elevation (m);

α   Kinetic energy correction coefficient, also called Coriolis coefficient taking into account the air–water flow properties ($\alpha = \dfrac{\int_0^{Y_{90}} \rho' \times V \times \frac{V^2}{2} \times dy}{\frac{1}{2} \times \left(\int_0^{Y_{90}} \rho' \times dy\right) \times \left(\frac{\int_0^{Y_{90}} \rho' \times V \times dy}{\int_0^{Y_{90}} \rho' \times dy}\right)^3}$)

β   Momentum correction coefficient, also called Boussinesq coefficient taking into account the air–water flow properties ($\beta = \dfrac{\int_0^{Y_{90}} \rho' \times V \times V \times dy}{\left(\int_0^{Y_{90}} \rho' \times dy\right) \times \left(\frac{\int_0^{Y_{90}} \rho' \times V \times dy}{\int_0^{Y_{90}} \rho' \times dy}\right)^2}$)

ΔH   Total head difference (m);

Λ   Air–water pressure correction coefficient introduced in the energy equation ($\Lambda = \dfrac{\int_0^{Y_{90}} V \times \left(\int_y^{Y_{90}} (1-C) \times dy' + (1-C) \times y\right) \times dy}{V_{mean} \times d^2}$)

μ   Dynamic viscosity (Pa.s) of water;

Ω   Air–water pressure correction coefficient introduced in the momentum equation ($\Omega = \dfrac{\int_0^{Y_{90}} \int_y^{Y_{90}} \rho \times (1-C) \times g \times dy' \times dy}{\frac{1}{2} \times \rho \times g \times d^2}$)

θ   Angle between longitudinal invert or pseudo-invert slope and horizontal;

ρ   Water density (kg/m^3);

ρ'   Two-phase fluid density (kg/m^3); in air–water flow: $\rho' = \rho \times (1-C)$;

τ_o Total boundary shear stress (Pa)

Subscript

c   Critical flow conditions;

IN   Influx into the control volume;

OUT   Outflux out of the control volume;

x   Longitudinal component;

90   Characteristic air–water property where the void fraction is C=0.90

1 Introduction

The interactions between supercritical flows and the atmosphere can lead to strong air–water mixing through the free-surface (Fig. 1). The free-surface aeration is caused by turbulence fluctuations acting next to the air–water free surface, through which air is continuously trapped and released in an uncontrolled fashion [20, 26, 40]. Even though the self-aerated free-surface flow is extremely complex, it can be treated as a homogenous air–water mixture, with the void fraction ranging from low values next to the bed to unity in the atmosphere [5, 9, 48]. The free-surface flow presents a very similar appearance irrespective of the bed roughness, and an un-informed visitor would not guess the invert type. This is illustrated in Fig. 1, comparing the self-aerated free-surface flows in natural and man-made environments.

In open channel flows, the dimensionless total drag may be expressed in the form of a Darcy-Weisbach friction factor and derived from both momentum and energy considerations, although the differences between the momentum and energy concepts have to be appreciated [38, 51]. In the following paragraphs, the theoretical expression of the total drag in self-aerated flows is derived based upon momentum conservation and from the energy concept in terms of the energy lost as the fluid moves. The present contribution aims to estimate the flow resistance in self-aerated flows based upon two different approaches, i.e. momentum and energy, for these complex multiphase flows although we acknowledge that there is a link between work and internal forces. This was undertaken through some theoretical development based upon an extension of traditional integral approaches to air–water flows, with the re-analyses of detailed air–water measurements in both prototype spillway chutes and large-size physical models. The applications were based upon the assumption that the pressure distribution remains hydrostatic, taking into account both the local density distributions and the non-uniform air–water velocity distributions.

2 Theoretical considerations

2.1 Momentum approach

The equation of conservation of momentum may be developed for self-aerated chute flows. For a fixed and rigid control volume (Fig. 2), the momentum principle states that the rate of change in momentum flux equals the sum of the forces applied to the control volume for a steady flow [23]. Considering a steady self-aerated flow, the momentum principle applied to the streamwise x-direction yields:

$$\int_{OUT} \rho' \times V \times V_x \times dA - \int_{IN} \rho' \times V \times V_x \times dA = \sum (Force)_x \tag{1}$$

where ρ' is the fluid density: $\rho' = \rho \times (1 - C)$ with ρ the water density and C the void fraction (i.e. neglecting the air density), V is the air–water velocity, A is the cross-section area normal to the main air–water flow direction and the subscript x refers to the streamwise component. In a stepped chute, Eq. (1) would typically be applied between two step edges, as illustrated in Fig. 2. The momentum principle must be applied to the control volume
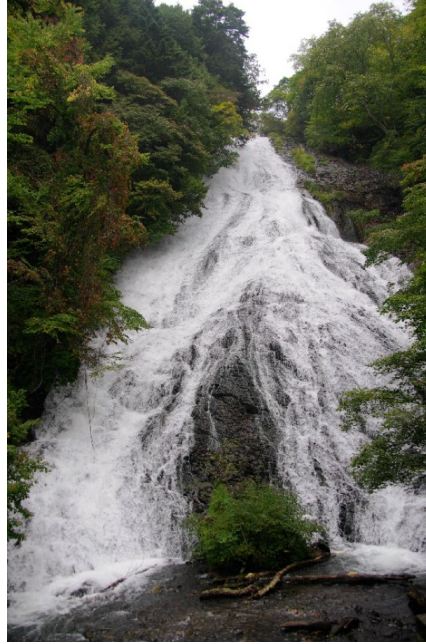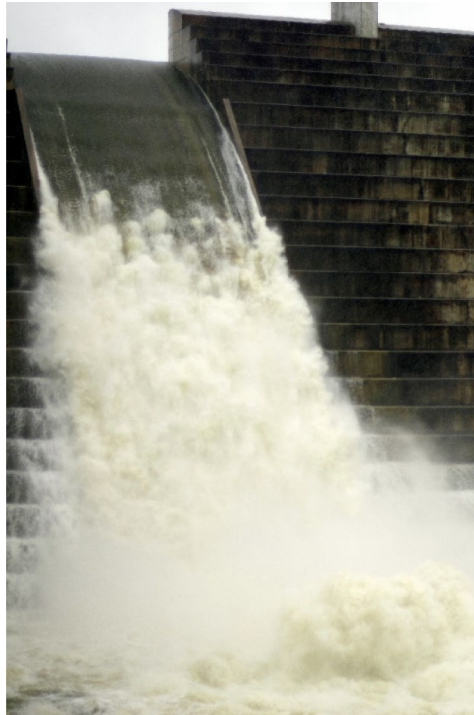
(A) 80 m high Yudaki Falls (Japan) on 7 October 2012

(B) North Pine Dam smooth spillway (Australia) in operation on 22 May 2009

Fig. 1 Self-aerated flows in Japan and Eastern Australia

(C) Hinze Dam Stage 3 stepped spillway (Australia) in operation on 23 March 2021

Fig. 1 (continued)

taking into account the air–water mixture properties. In a high-velocity self-aerated chute flow, the local void fraction C ranges from a very low value next to the invert to unity above the free-surface (Fig. 2), and the air and water flow as a homogeneous gas–liquid compressible mixture with no slip for $0 < C < 0.9$ [5, 47, 48]. In turn, the hydrostatic pressure distribution is non-linear as it accounts for the void fraction distribution, as illustrated in Fig. 2.

For a streamwise two-dimensional self-aerated chute flow (Fig. 2), the momentum flux entering/exiting the control volume may be expressed as:

$$\int_A \rho' \times V \times V \times dA = \int_0^{Y_{90}} \rho \times (1 - C) \times V \times V \times dy \times B = \beta \times \rho \times V_{mean} \times Q \quad (2)$$

with B the channel width, Y_{90} the characteristic distance where C = 0.90, Q the water discharge: $Q = V_{mean} \times d \times B$, V_{mean} the cross-sectional averaged velocity, β the momentum correction coefficient in self-aerated air–water flow defined as:

$$\beta = \frac{\int_0^{Y_{90}} \rho' \times V \times V \times dy}{\left(\int_0^{Y_{90}} \rho' \times dy\right) \times \left(\frac{\int_0^{Y_{90}} \rho' \times V \times dy}{\int_0^{Y_{90}} \rho' \times dy}\right)^2} = \frac{\int_0^{Y_{90}} \rho \times (1-C) \times V \times V \times dy}{\rho \times d \times V_{mean}^2} \tag{3}$$

and the equivalent clear-water depth d equals

$$d = \int_0^{Y_{90}} (1-C) \times dy \tag{4}$$

d represents the mean depth that would exist if the flow was without air entrainment [46]. For a monophase flow, $d = Y_{90}$, while $d < Y_{90}$ in self-aerated flows.

The application of the linear momentum equation to a skimming flow becomes:

$$\rho \times Q \times \left(\beta \times V_{mean}\right)_{OUT} - \rho \times Q \times \left(\beta \times V_{mean}\right)_{IN} = \left(\int_0^{Y_{90}} P \times B \times dy\right)_{IN}$$
$$- \left(\int_0^{Y_{90}} P \times B \times dy\right)_{OUT}$$
$$- F_{drag} + W \times \sin\theta \tag{5}$$

where P is the pressure, g is the gravity acceleration, F_{drag} is the total drag force, combining skin friction and form drag, and $W \times \sin\theta$ is the weight force component in the flow direction. Assuming a hydrostatic pressure distribution, i.e. the streamlines are parallel to each other, the pressure force per unit width acting at the upstream/downstream end of the control volume may be equal to:
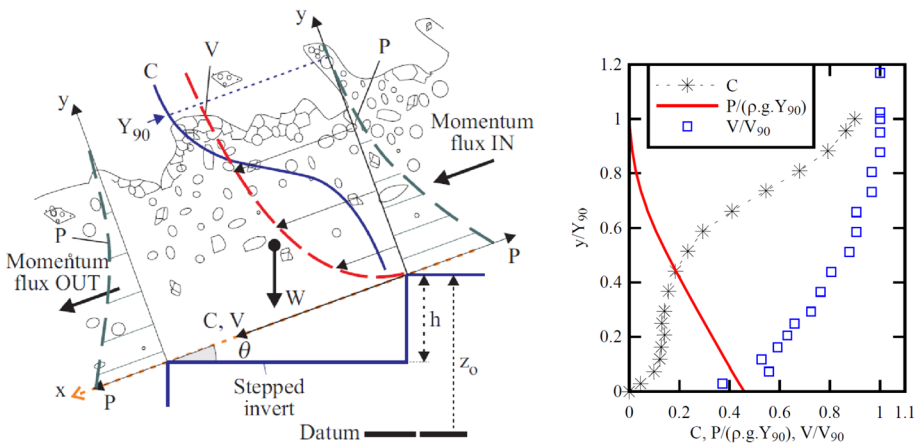
Fig. 2 Application of the momentum principle to a self-aerated chute flow control volume—inset (right): hydrostatic pressure, void fraction and interfacial velocity distributions in self-aerated skimming flow on a stepped chute (Data set UQ21 (Table 1), $d_c/h = 1.2$, $Re = 5.2 \times 10^5$, step edge 11, $C_{mean} = 0.35$)

$$\int_0^{Y_{90}} P \times dy = \int_0^{Y_{90}} \int_y^{Y_{90}} \rho \times (1 - C) \times g \times \cos\theta \times dy' \times dy = \frac{\Omega}{2} \times \rho \times g \times d^2 \times \cos\theta \quad (6)$$

where Ω is an air–water pressure correction coefficient, defined as:

$$\Omega = \frac{\int_0^{Y_{90}} \int_y^{Y_{90}} \rho \times (1 - C) \times g \times dy' \times dy}{\frac{1}{2} \times \rho \times g \times d^2} \quad (7)$$

For a rectangular channel, the weight force equals:

$$W = \int_{x_{in}}^{x_{out}} \int_0^{Y_{90}} \rho \times (1 - C) \times g \times B \times dy \times dx = \rho \times g \times d \times B \times (x_{OUT} - x_{IN}) \quad (8)$$

with d the average equivalent clear-water depth (Eq. 4) over the control volume, assumed in first approximation as: d $\approx$ (d$_{IN}$+d$_{OUT}$)/2, and the subscripts IN and OUT referring to the influx and outflow, respectively into and out of the control volume (Fig. 2 Left).

The linear momentum equation to a skimming flow may be rewritten as

$$\rho \times Q \times (\beta \times V_{mean})_{OUT} - \rho \times Q \times (\beta \times V_{mean})_{IN} = \left(\frac{\Omega}{2} \times \rho \times g \times d^2 \times \cos\theta \times B\right)_{IN}$$
$$- \left(\frac{\Omega}{2} \times \rho \times g \times d^2 \times \cos\theta \times B\right)_{OUT} \quad (9)$$
$$- F_{drag} + \rho \times g \times d \times B \times (x_{OUT} - x_{IN}) \times \sin\theta$$

in which the total drag force F$_{drag}$ may be expressed as a function of the total boundary shear stress τ_o, hence in terms of the Darcy–Weisbach friction factor f:

$$F_{drag} = \tau_o \times P_w \times (x_{OUT} - x_{IN}) = \frac{f}{8} \times \rho \times V_{mean}^2 \times P_w \times (x_{OUT} - x_{IN}) \quad (10)$$

with P$_w$ the wetted perimeter, which could be approximated as P$_w \approx$ B for a wide channel.

The momentum equation applied to gradually-varied flow conditions provides an expression of the total drag:

$$F_{drag} = \frac{f}{8} \times \rho \times V_{mean}^2 \times P_w \times (x_{OUT} - x_{IN})$$
$$= \rho \times Q \times (\beta \times V_{mean})_{IN} - \rho \times Q \times (\beta \times V_{mean})_{OUT}$$
$$+ \left(\frac{\Omega}{2} \times \rho \times g \times d^2 \times \cos\theta \times B\right)_{IN}$$
$$- \left(\frac{\Omega}{2} \times \rho \times g \times d^2 \times \cos\theta \times B\right)_{OUT}$$
$$+ \rho \times g \times d \times B \times (x_{OUT} - x_{IN}) \times \sin\theta \quad (11)$$

For completeness, at uniform equilibrium down a wide steep chute (P$_w \approx$ B, D$_H \approx$ 4$\times$d), the momentum principle may be simplified into

$$F_{drag} = \rho \times g \times d \times B \times (x_{OUT} - x_{IN}) \times \sin\theta \quad (12a)$$

In dimensionless terms:

$$f = \frac{F_{drag}}{\frac{\rho}{8} \times V_{mean}^2 \times P_w \times (x_{OUT} - x_{IN})} \approx \frac{8 \times g \times d \times \sin\theta}{V_{mean}^2} \qquad (12b)$$

Note the absence of pressure and velocity corrections coefficients in Eq. (12), because the momentum fluxes, and the pressure forces, cancelled out in the momentum equation at uniform equilibrium. Noteworthy, the concept of "uniform equilibrium" may be linked to the selection of the most relevant air–water parameters. For example, experimental data showed that the longitudinal distributions of depth-averaged void fraction C_{mean} and velocity V_{mean} reach relatively rapidly some pseudo-equilibrium asymptote [27, 46, 50], but other properties, such as bubble count rate and interfacial area, require a much longer chute length, rarely encountered in laboratory [21, 50]. Further, the notion of uniform equilibrium and flow resistance in skimming flows may not be unique functions of flow rate and stepped chute geometry. Several studies argued that the form drag process on stepped chutes may present several excitation modes, being linked to the inflow conditions [14, 15].

2.2 Energy approach

A comparable development in terms of work and energy may be derived based upon the work-energy theorem [31, 41]. Considering the control volume shown in Fig. 2 (Left), the variation of power associated with kinetic energy is associated to both external and internal forces.

From the equation of motion, each term is multiplied by the corresponding velocity component [41]. The rate of change in kinetic energy of the system equals for a steady flow and a fixed and rigid control volume:

$$\dot{KE} = \int_{OUT} \rho' \times V \times \frac{V^2}{2} \times dA - \int_{IN} \rho' \times V \times \frac{V^2}{2} \times dA \qquad (13)$$

where KE is the kinetic, the over-dot (•) indicates the rate of kinetic energy change [30, 36]. Introducing the kinetic energy correction coefficient in air–water flow:

$$\alpha = \frac{\int_0^{Y_{90}} \rho' \times V \times \frac{V^2}{2} \times dy}{\frac{1}{2} \times \left(\int_0^{Y_{90}} \rho' \times dy\right) \times \left(\frac{\int_0^{Y_{90}} \rho' \times V \times dy}{\int_0^{Y_{90}} \rho' \times dy}\right)^3} = \frac{\int_0^{Y_{90}} \rho \times (1 - C) \times V \times \frac{V^2}{2} \times dy}{\frac{1}{2} \times \rho \times (1 - C_{mean}) \times Y_{90} \times V_{mean}^3} \qquad (14)$$

the kinetic energy flux entering/exiting the control volume may be rewritten as

$$\frac{1}{B} \times \int_A \rho' \times V \times \frac{V^2}{2} \times dA = \alpha \times \frac{1}{2} \times \rho \times V_{mean}^3 \times d \qquad (15)$$

with d the equivalent clear-water depth (Eq. 4).

Similarly, the rate of change in works associated to conservative forces (weight and pressure) may be expressed as:

$$\dot{U} = \int\limits_{OUT} \rho' \times V \times \left(\frac{P}{\rho'} + g \times z \right) \times dA - \int\limits_{IN} \rho' \times V \times \left(\frac{P}{\rho'} + g \times z \right) \times dA \qquad (16)$$

where U is the works associated to conservative forces and z is the vertical elevation positive upwards. Assuming a hydrostatic pressure gradient, the pressure distribution fulfills:

$$P(y) = \int\limits_{y}^{Y_{90}} \rho \times (1 - C) \times g \times \cos\theta \times dy' \qquad (17)$$

Equation (17) is shown in Fig. 2 (Inset) for an experimental data set in a skimming flow on a stepped chute. The results illustrated the effect of self-aeration on the pressure distribution.

The energy flux entering/exiting the control volume per unit width may then be expressed as:

$$\frac{1}{B} \times \int\limits_{A} \rho' \times V \times \left(\frac{P}{\rho'} + g \times z \right) \times dA$$
$$= \int\limits_{0}^{Y_{90}} V \times \left(\int\limits_{y}^{Y_{90}} \rho \times (1 - C) \times g \times \cos\theta \times dy' + \rho \times (1 - C) \times g \times y \times \cos\theta \right) \times dy + \rho \times g \times z_o \times V_{mean} \times d \qquad (18)$$

with z_o the invert elevation. Defining a different air–water pressure correction coefficient Λ:

$$\Lambda = \frac{\int\limits_{0}^{Y_{90}} V \times \left(\int\limits_{y}^{Y_{90}} (1 - C) \times dy' + (1 - C) \times y \right) \times dy}{V_{mean} \times d^2} \qquad (19)$$

the flux of conservative forces entering/exiting the control volume becomes for a streamwise two-dimensional air–water chute flow (Fig. 2):

$$\frac{1}{B} \times \int\limits_{A} \rho' \times V \times \left(\frac{P}{\rho'} + g \times z \right) \times dA = \rho \times g \times V_{mean} \times d \times \left(\Lambda \times d \times \cos\theta + z_o \right) \qquad (20)$$

Assimilating the opposite of the works associated to weight and pressure (conservative forces) to potential energies, the work-energy theorem leads to the Bernoulli equation. Introducing the total head loss ΔH, the combination of Eqs. (15) and (20) give the total head loss across the control volume

$$\Delta H = H_{OUT} - H_{IN}$$
$$= \left(\Lambda \times d \times \cos\theta + z_o + \alpha \times \frac{V_{mean}^2}{2 \times g} \right)_{OUT} - \left(\Lambda \times d \times \cos\theta + z_o + \alpha \times \frac{V_{mean}^2}{2 \times g} \right)_{IN} \qquad (21)$$

where the terms in brackets represent the total head.

By extension over a short distance ∂x, one may relate the slope of the total head line $S_f = -\partial H/\partial x$ to the Darcy–Weisbach friction factor combining both skin friction and form drag turbulent losses:

$$\frac{\partial}{\partial x}\left(\Lambda \times d \times \cos\theta + z_o + \alpha \times \frac{V_{mean}^2}{2 \times g}\right) = -f \times \frac{1}{D_H} \times \frac{V_{mean}^2}{2 \times g} \qquad (22)$$

with D_H the hydraulic diameter. In Eq. (22), the right handside term represents the power dissipated by the internal viscous forces, while the left handside term is the rate of change of mechanical energy. One notes that Eq. (22) is basically a broad form of the backwater equation [25], and the above development extends the reasoning of Takahashi and Ohtsu [45].

Finally, the differences caused by the two-phase flow nature of the flow, between the corrected-equation solution, i.e. Eqs. (9) and (22), and the standard hydraulic solutions, are the introduction of the pressure correction coefficient Ω and Λ , which are unity in mono-phase flows on flat slope and hydrostatic pressure distributions, and the expressions of the velocity correction coefficients β and α, i.e. Eqs. (3) and (14) respectively, which differ the traditional correction relationships (e.g. [13, 18]).

3 Application

The present developments were applied to a number of detailed air–water flow data sets (Table 1). The data sets included both detailed void fraction and interfacial velocity measurements in self-aerated gradually-varied smooth and stepped chute flows, including prototype data. Table 1 lists the flow conditions corresponding to the data sets, which encompassed detailed air–water flow measurements, with both detailed void fraction and interfacial velocity distributions recorded at several closely-spaced longitudinal locations along a channel, for a given discharge and boundary treatment. The data sets were further obtained at relatively large Reynolds numbers (Table 1, 7th column), since scale effects in air water self-aerated flows have been well-acknowledged in the literature [9, 19, 29, 40, 48]. For the stepped chute data, the air–water flow properties were measured at each step edge downstream of the air entrainment inception region. For a given flow rate, the air–water velocity and pressure correction coefficients varied with longitudinal distance, in response to changes in the interfacial velocity distributions and in the void fraction distributions. Some experimental data are presented in Fig. 3 (i.e. velocity and pressure correction coefficients), Fig. 4 (i.e. friction factor) and Fig. 5 (i.e. residual energy). Figure 3 presents the velocity and pressure correction coefficients at each measurement location on smooth chutes and at each step edge on stepped chute, as functions of the local depth-averaged void fraction C_{mean}. In Fig. 4, the friction factor data was calculated over the air–water self-aerated flow region, i.e. the presented data are some spatial averaged values. Note that the parameters are plotted as functions of the mean void fraction C_{mean}, because there is a self-similarity of all void fraction profiles based upon C_{mean}, as previously reported in the literature [9, 46, 47, 49]. Another relevant parameter may be the Reynolds number, since scale effects in air water self-aerated flows have been well-acknowledged in the literature, for that reason, the present analysis focused on the selection and use of detailed experimental data sets obtained at large Reynolds numbers (Table 1, 7th column).

**Table 1** Detailed air–water data sets in smooth and stepped chutes re-analysed in the current study

Data set	References	θ (°)	B (m)	q (m²/s)	V_{90} (m/s)	Re	Geometry	Instrumentation
JL53	Jevdjevich and Levin [28]	> 45	5.35	0.73 & 1.94	16–30	2.9×10^6 and 7.7×10^6	Prototype masonry chute	N/A
Aviemore	Cain [4]	45	90	2.23 & 3.16	18–22	0.89×10^7 and 1.3×10^7	Prototype smooth concrete chute	Dual-tip phase-detection probe ($\varnothing = 1$ mm)
UC88	Chanson [6]	52.3	0.25	0.27 & 0.36	11–16	0.86×10^6 and 1.15×10^6	Smooth perspex chute	Dual-tip phase-detection probe ($\varnothing = 0.2$ mm)
UQ97	Chanson [10]	4.0	0.50	0.15	3.8–5.0	6.0×10^5	Smooth timber chute	Dual-tip phase-detection probe ($\varnothing = 0.025$ mm)
UQ21	Arosquipa Nina et al. [1, 2]	45	0.985	0.07 to 0.20	2.5–4.7	2.8×10^5 to 8.0×10^5	Stepped chute (h=0.1 m, horizontal steps)	Dual-tip phase-detection probe ($\varnothing = 0.25$ mm)

B, chute width; *h*, step height; *q*, unit water discharge; *Re*, Reynolds number defined in terms of hydraulic diameter; V_{90} characteristic velocity at the location where C=0.90; θ angle between invert or pseudo-invert slope and horizontal; *N/A*: not available
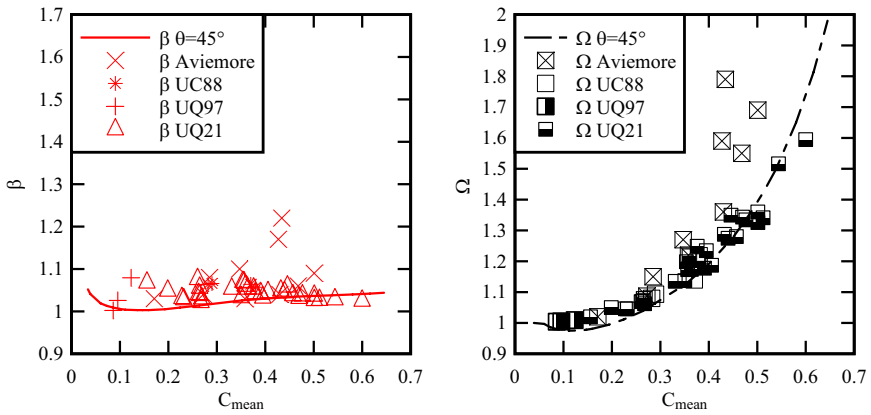
(A, Left) Momentum correction coefficient β

(B, Right) Pressure correction coefficient Ω
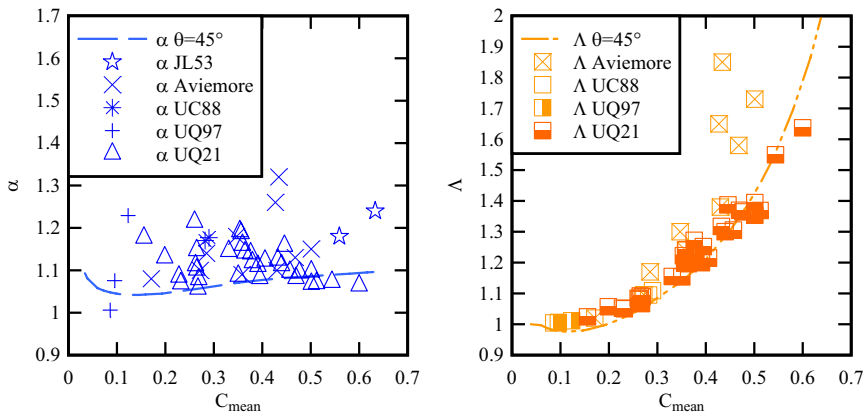
(C, Left) Kinetic energy correction coefficient α

(D, Right) Pressure correction coefficient Λ

Fig. 3 Variations of correction coefficients β, α, Ω and Λ as functions of the depth-averaged void fraction C_{mean} in self-aerated chutes flows: comparison between experimental data (Table 1) and calculations for θ = 45°—Calculations conducted assuming a 1/6th power law velocity distribution and void fraction profiles following an advective diffusion model

The variations of the coefficients β, α, Ω and Λ (i.e. Eqs. (3, 15, 7, 18) respectively) are presented extensively in Appendix and typical results are shown in Fig. 3 as functions of the depth-averaged void fraction C_{mean}. In Fig. 3, the calculations were conducted for θ = 45° assuming a 1/6th interfacial velocity power law (i.e. N = 6) observed in prototype and model [5, 10], hydrostatic pressure distributions taking into account self-aeration, and void fraction profiles that followed an advective diffusion model [16]. Overall, the calculations indicated that the correction coefficients β, α,

Ω and Λ were primarily affected by the mean air content C_{mean}, but little impacted by the chute slope and velocity power law exponent, within $4° < \theta < 60°$ and $6 < N < 10$ (Calculations not shown), thus justifying the result presentation for $N = 6$ only. Figure 3 further shows a comparison between the calculations and experimental observations (Table 1). For both calculations and experimental data, the pressure correction coefficients Ω and Λ presented a marked effect caused by self-aeration, reaching about two for $C_{mean} = 0.65$, while presenting a minimum about one, or slightly less, for $C_{mean} \sim 0.11$ (Fig. 3). Some data scatter is seen in Fig. 3A and C, possibly linked to differences in instrumentation and experimental conditions between the data sets, collected over several decades.

Finally, the above developments assumed that the pressure gradient was hydrostatic. When the pressure gradient is not hydrostatic, e.g. in a flip bucket downstream of a steep spillway, the expression of the pressure distribution must be modified to account for the non-hydrostatic pressure.
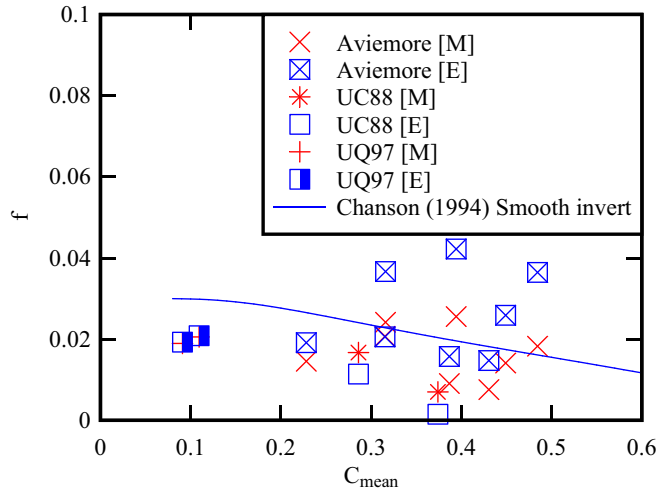
3.1 Friction factor

The experimental data sets were re-analysed in terms of the friction factor f. Two estimates were derived from momentum [M] and energy [E} considerations, i.e. Eqs. (11) and (22) respectively, for these complicated self-aerated flows. The data are presented in Fig. 4 as a function of the depth-averaged void fraction $C_{mean} = 1—d/Y_{90}$.

First, the data showed a greater Darcy-Weisbach friction factor for the stepped chutes, as expected because of the step macro-roughness [7, 39]. Second, all the data showed some reduction in friction factor with increasing depth-averaged void fraction for a given chute configuration. The finding is in line with the literature on self-aerated flows [8, 12, 13, 28, 46]. (For completeness, the Aviemore Dam data set showed the same trend for a given discharge in Fig. 4A [46]). The drag reduction is believed to be linked to a combination of mechanisms including a void fraction defect next to the invert, intense bubble-turbulence interactions and some modification of the turbulent shear stress field [8, 33, 37]. Third, the momentum and energy results were close, although the data showed subtle differences in the friction factor estimates depending upon the approach (Fig. 4. This was expected, because the momentum approach yields a dimensionless total drag; $f \propto F_{drag}$ (Eq. 10), while the energy considerations give a dimensionless total energy line slope: $f \propto S_f$ (Eq. 22). If the friction factor is used for energy dissipation calculations, the latter approach should be used, while the former would be applied to estimate the forces acting on the invert.

Finally, the above developments presented the derivation of the friction factor based upon an integral approach, i.e. Eqs. (11) and (22) respectively. Another momentum-based approach may be based upon the analyses of the velocity profiles [35, 42, 43]. The skin friction is derived from the law of the wall [3], and the approach has been recently extended to heterogeneous roughness [38]. In another method, the skin friction of canonical flows may be developed based upon momentum considerations and the distributions of Reynold stress [22].

3.2 Residual head

For dam spillway design, the residual energy at the chute toe is a key parameter, e.g. to dimension a downstream stilling structure. The residual head may be estimated based upon

(A) Smooth chute data - Comparison with drag reduction correlation (Chanson 1994b)
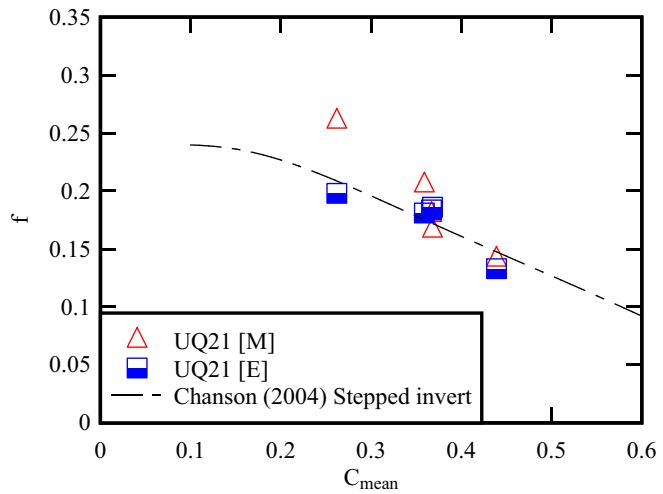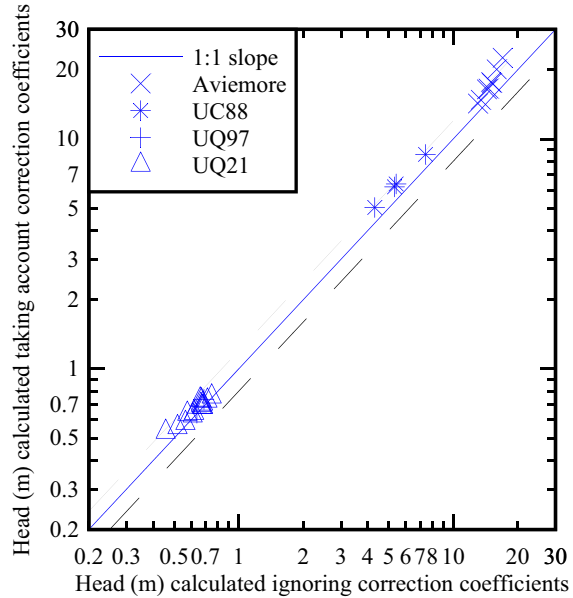

(B) Stepped chute data - Comparison with drag reduction correlation (Chanson 2004)

Fig. 4 Friction factor in self-aerated chute data sets (Table 1) as a function of the depth-averaged void fraction C_{mean}—Comparison between momentum [M] and energy [E] considerations (i.e. Eqs. (11) and (22) respectively)—The smooth and stepped chute data are further compared to drag reduction correlations

the air–water flow properties taking into account the non-uniform air–water velocity profiles and air–water pressure distributions:

Fig. 5 Calculation of residual head H_{res} at the downstream end of self-aerated chutes (Table 1)—Comparison of estimations with and without air–water pressure and velocity correction coefficients: i.e. Eq. (23) [vertical axis] versus Eq. (24) [horizontal axis]—Dashed black lines at ± 20%

with α and Λ being some air–water kinetic energy and pressure correction coefficients respectively (Eqs. 15 and 18 respectively), $V_{mean} = Q/A$ and A the equivalent clear-water cross-section area ($A = B \times d$ for a rectangular chute). The present calculations of residual head H_{res} (Eq. 23) were compared to the more "traditional" approach, ignoring the air–water pressure and velocity correction coefficients, for the same data sets. That is, assuming that the residual head may be approximated as:

$$H_{res} = d \times \cos\theta + \frac{V_{mean}^2}{2 \times g} \qquad (24)$$

implicitly assuming α = 1 and Λ = 1. The comparative data are reported in Fig. 5 with the more traditional estimates (Eq. (24)) on the horizontal axis. Note that the data are presented in a dimensional form in Fig. 5 to emphasise the range of the data sets. Overall, the residual head was systematically under-estimated, by 10.1% in average, using the traditional method (Eq. 24) and ignoring the air–water pressure and velocity correction coefficients. The present result was obtained for both smooth and stepped chutes, and it is close to earlier observations on stepped spillways [45]. Simply, the absence of correction coefficients leads to an over-estimation of the rate of energy dissipation, compared to the detailed calculations using the relevant air–water velocity and pressure correction coefficients, based upon detailed air–water flow data sets. In practice, Fig. 3A, B, C and D provide analytical solutions (thick lines) of the correction coefficients that may be used as design guidelines in first approximation, with calculations for other slopes reported in Appendix .

$$H_{res} = \frac{\int_A \rho' \times V \times \left(\frac{P}{\rho'} + g \times z + \frac{V^2}{2}\right) \times dA}{\rho \times g \times V_{mean} \times A} = \Lambda \times d \times \cos\theta + \alpha \times \frac{V_{mean}^2}{2 \times g} \qquad (23)$$

4 Conclusion

In self-aerated free-surface flows, experimental observations without detailed air–water flow measurements tend to over-estimate the flow depth, to under-estimate the flow velocity, and to grossly over-estimate the flow resistance and rate of energy dissipation on stepped chutes [17, 24]. Detailed air–water flow measurements constitute a basic requirement for reliable estimates of flow resistance and energy losses [11, 32, 46]. In the current work, the friction factor f is derived from momentum and energy considerations for complex self-aerated flows. In the momentum equation, f represents a dimensionless total drag. In the energy equation, f is a dimensionless expression of the rate of energy dissipation. Both approaches necessitate to consider the non-uniform velocity and pressure distributions, and the air–water kinetic energy and pressure correction coefficients were derived theoretically herein.

The friction factor f and residual head H_{res} were estimated for smooth and stepped self-aerated chute flows, including prototype (and large-size model) data (Table 1). Both the momentum and energy approaches yielded close results in terms of the friction factor. Based upon the same detailed air–water flow data sets, the absence of correction coefficients was found to under-estimate the residual head and to over-estimate the rate of energy dissipation, compared to the detailed calculations using the relevant air–water velocity and pressure correction coefficients. The finding has some basic design implications. Since professional engineers must be conservative, the calculations procedure must account for the pressure and velocity correction coefficients taking into account the air–water flow properties. The trendlines in Fig. 3, drawn for $\theta = 45°$, could be used to estimate the coefficients as functions of the depth-averaged void fraction, when the detailed air–water flow properties are not measured.

Appendix

Calculations of air–water kinetic and pressure correction coefficients for a range of invert slopes and velocity power law exponent

The variations of the air–water kinetic energy and pressure coefficients β, α, Ω and Λ (i.e. Eqs. (3), (15), (7), (18) respectively) were performed for several invert slopes $20° < \theta < 55°$ assuming 1/N interfacial velocity power law, with $6 < N < 10$, and void fraction profiles that followed an advective diffusion model [16]. The results are included in Table 2.

Table 2 Variations of dimensionless correction coefficients β, α, Ω and Λ as functions of the depth-averaged void fraction C_{mean} in self-aerated chutes flows for $30° < θ < 45°$— Calculations conducted assuming a 1/Nh power law velocity distribution and void fraction profiles following an advective diffusion model

θ (°)	C_{mean}	N	β	α	Ω	Λ
45	0.039	8	1.032	1.056	1.038	1.038
45	0.060	8	1.010	1.034	0.997	0.997
45	0.159	8	0.994	1.018	0.981	0.983
45	0.264	8	1.005	1.031	1.039	1.045
45	0.398	8	1.020	1.048	1.188	1.202
45	0.538	8	1.027	1.058	1.497	1.526
45	0.616	8	1.031	1.063	1.813	1.853
30	0.039	8	1.032	1.056	1.038	1.038
30	0.060	8	1.010	1.034	0.997	0.997
30	0.099	8	0.997	1.021	0.976	0.977
30	0.159	8	0.994	1.018	0.981	0.983
30	0.264	8	1.005	1.031	1.039	1.045
30	0.398	8	1.020	1.048	1.188	1.202
30	0.486	8	1.025	1.055	1.357	1.380
45	0.039	10	1.028	1.044	1.038	1.038
45	0.060	10	1.006	1.022	0.997	0.997
45	0.099	10	0.993	1.009	0.976	0.977
45	0.159	10	0.990	1.006	0.981	0.983
45	0.264	10	1.000	1.018	1.039	1.044
45	0.398	10	1.015	1.034	1.188	1.199
45	0.486	10	1.020	1.040	1.357	1.375
45	0.538	10	1.022	1.042	1.497	1.520
45	0.616	10	1.025	1.046	1.813	1.845
45	0.034	6	1.052	1.093	1.061	1.061
45	0.039	6	1.041	1.081	1.038	1.038
45	0.060	6	1.019	1.058	0.997	0.997
45	0.073	6	1.013	1.052	0.986	0.987
45	0.086	6	1.009	1.048	0.980	0.981
45	0.099	6	1.006	1.045	0.976	0.977
45	0.111	6	1.004	1.043	0.975	0.976
45	0.136	6	1.003	1.042	0.976	0.978
45	0.147	6	1.003	1.042	0.978	0.980
45	0.159	6	1.003	1.043	0.981	0.984
45	0.193	6	1.005	1.045	0.994	0.998
45	0.224	6	1.009	1.050	1.011	1.017
45	0.264	6	1.014	1.056	1.039	1.047
45	0.352	6	1.026	1.071	1.126	1.141
45	0.398	6	1.030	1.077	1.188	1.207
45	0.451	6	1.034	1.082	1.280	1.306
45	0.486	6	1.036	1.085	1.357	1.387
45	0.513	6	1.037	1.087	1.425	1.459
45	0.538	6	1.038	1.089	1.497	1.535
45	0.580	6	1.040	1.092	1.650	1.696
45	0.616	6	1.042	1.095	1.813	1.865
45	0.645	6	1.044	1.097	1.980	2.039
55	0.034	6	1.051	1.092	1.059	1.059
55	0.047	6	1.029	1.068	1.016	1.016

Table 2 (continued)

θ (°)	C_{mean}	N	β	α	Ω	Λ
55	0.060	6	1.019	1.058	0.997	0.997
55	0.086	6	1.009	1.048	0.980	0.981
55	0.111	6	1.004	1.043	0.975	0.976
55	0.159	6	1.003	1.043	0.981	0.984
55	0.264	6	1.014	1.056	1.039	1.047
55	0.352	6	1.026	1.071	1.126	1.141
55	0.486	6	1.036	1.085	1.357	1.387
55	0.580	6	1.040	1.092	1.650	1.696
55	0.645	6	1.044	1.097	1.980	2.039
55	0.034	8	1.043	1.067	1.059	1.059
55	0.047	8	1.020	1.045	1.016	1.016
55	0.060	8	1.010	1.034	0.997	0.997
55	0.086	8	1.000	1.024	0.980	0.981
55	0.111	8	0.996	1.019	0.975	0.976
55	0.159	8	0.994	1.018	0.981	0.983
55	0.264	8	1.005	1.031	1.039	1.045
55	0.352	8	1.016	1.043	1.126	1.137
55	0.486	8	1.025	1.055	1.357	1.380
55	0.580	8	1.029	1.060	1.650	1.685
55	0.645	8	1.032	1.064	1.980	2.025
55	0.034	10	1.038	1.055	1.059	1.059
55	0.047	10	1.016	1.032	1.016	1.016
55	0.060	10	1.006	1.022	0.997	0.997
55	0.086	10	0.996	1.012	0.980	0.980
55	0.111	10	0.991	1.007	0.975	0.976
55	0.159	10	0.990	1.006	0.981	0.983
55	0.264	10	1.000	1.018	1.039	1.044
55	0.352	10	1.011	1.029	1.126	1.135
55	0.486	10	1.020	1.040	1.357	1.375
55	0.580	10	1.023	1.044	1.650	1.678
55	0.645	10	1.026	1.048	1.980	2.017

References

1. Arosquipa Nina Y., Shi, R., Wüthrich, D., and Chanson, H. (2021). Intrusive and Non-Intrusive Air-Water Measurements on Stepped Spillways with inclined steps: a Physical Study on Air Entrainment and Energy Dissipation. Hydraulic Model Report No, School of Civil Engineering, The University of Queensland, Brisbane, Australia, 259 p. 8

2. Arosquipa Nina Y, Shi R, Wüthrich D, Chanson H (2022) Air–Water flows and head losses on stepped spillways with inclined steps. J Irrig Drain Eng 148(11):04022037. https://doi.org/10.1061/(ASCE)IR.1943-4774.0001701

3. Bradshaw, P. (1971). "An Introduction to Turbulence and its Measurement." *Pergamon Press*, Oxford, UK, The Commonwealth and International Library of Science and technology Engineering and Liberal Studies, Thermodynamics and Fluid Mechanics Division, 218 pages.

4. Cain P (1978) Measurements within self-aerated flow on a large spillway. Ph.D. Thesis, Ref. 78–18, Dept. of Civil Engrg., Univ. of Canterbury, Christchurch, New Zealand

5. Cain P, Wood IR (1981) Measurements of self-aerated flow on a spillway. Jl Hyd Div 107(11):1425–1444

6. Chanson H (1988) A study of air entrainment and aeration devices on a spillway model. Ph.D. thesis, Dept. of Civil Engrg., University of Canterbury, New Zealand

7. Chanson H (1994) Hydraulics of skimming flows over stepped channels and spillways. J Hydraul Res 32(3):445–460. https://doi.org/10.1080/00221689409498745

8. Chanson H (1994) Drag reduction in open channel flow by aeration and suspended load. J Hydraul Res 32(1):87–101. https://doi.org/10.1080/00221689409498791

9. Chanson H (1997) Air bubble entrainment in free-surface turbulent shear flows. Academic Press, London, p 401

10. Chanson H (1997) Air bubble entrainment in open channels. Flow structure and bubble size distributions. Int J Multiph Flow 23(1):193–203. https://doi.org/10.1016/S0301-9322(96)00063-8

11. Chanson H (2001) The Hydraulics of stepped chutes and spillways. Balkema, Lisse

12. Chanson H (2004) Drag reduction in skimming flow on stepped spillways by aeration. J Hydraul Res 42(3):316–322

13. Chanson, H (2004b) The Hydraulics of Open Channel Flow An Introduction. *Butterworth-Heinemann*, 2, Oxford, UK, 630

14. Chanson H (2006) Hydraulics of skimming flows on stepped chutes: the effects of inflow conditions? J Hydraul Res 44(1):51–60

15. Chanson H, Bung D, Matos J (2015) Stepped spillways and cascades. In: Chanson H (ed) Energy dissipation in hydraulic structures. IAHR Monograph CRC Press, Taylor & Francis Group, Leiden, pp 45–64

16. Chanson H, Toombes L (2002) Air-water flows down stepped chutes: turbulence and flow structure observations. Int J Multiph Flow 28(11):1737–1761. https://doi.org/10.1016/S0301-9322(02)00089-7

17. Chanson H, Yasuda Y, Ohtsu I (2002) Flow resistance in skimming flows and its modelling. Can J Civ Eng 29(6):809–819. https://doi.org/10.1139/L02-083

18. Chow VT (1959) Open channel hydraulics. McGraw-Hill, New York

19. Ervine DA (1998) Air Entrainment in Hydraulic Structures: a Review. Proc Inst Civ Eng Water Marit Energy UK 130:142–153

20. Ervine DA, Falvey HT (1987) Behaviour of turbulent water jets in the atmosphere and in plunge pools. Proc Inst Civ Eng 83:295–314 (**Discussion: Part 2, Mar. June 1988, 85, pp. 359–363**)

21. Felder S, Chanson H (2009) Turbulence, dynamic similarity and scale effects in high-velocity free-surface flows above a stepped chute. Exp Fluids 47(1):1–18. https://doi.org/10.1007/s00348-009-0628-3

22. Fukagata K, Iwamoto K, Kasagi N (2002) Contribution of Reynolds Stress Distribution to the Skin Friction in Wall-bounded Flows. Phys Fluids 14(11):L73–L77

23. Gerhart, PM, Gross, RJ, and Hochstein, JI (1992) Fundamentals of Fluid Mechanics." *AddisonWesley Publ*, Reading MA, USA, 2nd edition, 983

24. G Halbronn (1952) Etude de la Mise en Régime des Ecoulements sur les Ouvrages à Forte Pente. Applications au Problème de l'Entraînement d'Air. Study of the Setting up of the Flow Regime on High Gradient Structures. Application to Air Entrainment Problem. *Journal La Houille Blanche*, No. 1, pp. 21–40; No. 3, pp. 347–371; No. 5, pp. 702–722 (in French)

25. Henderson FM (1966) Open channel flow. MacMillan Company, New York

26. Hino, M (1961) On the Mechanism of Self-Aerated Flow on Steep Slope Channels. Applications of the Statistical Theory of Turbulence" *Proc IAHR Congress*, Dubrovnick, Yugoslavia, 123–132
27. Gonzalez CA (2005) An Experimental Study of Free-Surface Aeration on Embankment Stepped Chutes. Ph.D. thesis, Department of Civil Engineering, The University of Queensland, Brisbane, Australia
28. V Jevdjevich, L Levin (1953). Entrainment of air in flowing water and technical problems connected with it. Proc. 5th IAHR Congress, IAHR-ASCE, Minneapolis, USA, pp. 439–454
29. Kobus H (1984) Scale Effects in Modelling Hydraulic Structures. Proceedings International Symposium on Scale Effects in Modelling Hydraulic Structures, IAHR, Esslingen, Germany
30. Liggett JA (1993) Critical depth, velocity profiles and averaging. J Irrig Drain Eng 119(2):416–422
31. Liggett JA (1994) Fluid mechanics. McGraw-Hill, New York
32. J Matos, I Meireles (2014). Hydraulics of stepped weirs and dam spillways: engineering challenges, labyrinths of research. In: Hydraulic Structures and Society—Engineering Challenges and Extremes, The University of Queensland, Brisbane, Australia, Proceedings of the 5th IAHR International Symposium on Hydraulic Structures (ISHS2014), 25–27 June 2014, Brisbane, Australia, H. Chanson and L. Toombes Editors, 30 https://doi.org/10.14264/uql.2014.11
33. Marié JL (1987) A Simple analytical formulation for microbubble drag reduction. PCH 8(2):213–220
34. Meireles I (2011) Hydraulics of stepped chutes: experimental-numerical-theoretical study. Ph.D. thesis, University of Aveiro, Portugal
35. C M Millikan (1938). Critical Discussion of turbulent flows in channels and circular tubes. In: Proc. 5th International Congress of Applied Mechanics, Wiley, New York, USA, pp. 386–392
36. Montes JS (1998) Hydraulics of open channel flow. ASCE Press, New York, p 697
37. Murai Y (2014) Frictional drag reduction by bubble injection. Exp Fluids 55:28. https://doi.org/10.1007/s00348-014-1773-x
38. Nikora V, Stoesser T, Cameron SM, Stewart M, Papadopoulos K, Ouro P, McSherry R, Zampiron A, Marusic I, Falconer RA (2019) Friction factor decomposition for rough-wall flows: theoretical background and application to open-channel flows. J Fluid Mech 872:626–644. https://doi.org/10.1017/jfm.2019.344
39. Rajaratnam N (1990) Skimming flow in stepped spillways. J Hydraul Eng 116(4):587–591
40. Rao NSL, Kobus HE (1974) Characteristics of self-aerated free-surface flows water and waste water/current research and practice. Eric Schmidt Verlag, Berlin
41. Rouse H (1959) Advanced mechanics of fluids. John Wiley, New York, p 444
42. Rouse H (1965) Critical analysis of open-channel resistance. J Hydraul Div 91(HY4):1–25
43. Schlichting H (1979) Boundary layer theory, 7th edn. McGraw-Hill, New York
44. T W Sturm (2001) Open channel hydraulics. McGraw Hill, Boston, USA, Water resources and environmental engineering series, 493
45. Takahashi M, Ohtsu I (2012) Aerated flow characteristics of skimming flow over stepped chutes. J Hydraul Res 50(4):427–434. https://doi.org/10.1080/00221686.2012.702859
46. Wood IR (1983) Uniform region of self-aerated flow. J Hydraul Eng 109(3):447–461
47. I R Wood (1984). Air Entrainment in High Speed Flows. In: Proc International Symposium on Scale Effects in Modelling Hydraulic Structures, H. Kobus editor IAHR, Esslingen, Germany, paper 41, 7
48. I R Wood (1985). Air water flows. In: Proc. 21st IAHR Congress, Melbourne, Australia, Keynote address, pp 18–29
49. Wood IR (1991) Air entrainment in free-surface flows. IAHR hydraulic structures design manual, hydraulic design considerations. Balkema Publ., Rotterdam, p 149
50. Yasuda Y, Chanson H (2003) Micro and macro scopic study of two phase flow on a stepped chute. In: Proc 30th IAHR Biennial Congress, Thessaloniki, Greece, J Ganoulis and P Prinos Editors, pp. 695–702
51. Yen BC (2002) Open channel flow resistance. J Hydraul Eng ASCE 128(1):20–39